The Journal of cells, molecules, systems and technologies

IMMUNOLOGY ORIGINAL ARTICLE

The Warburg effect in mycobacterial granulomas is dependent on the recruitment and activation of macrophages by interferon-γ

Rui Appelberg,[1] Diana Moreira,[1,2] Palmira Barreira-Silva,[3,4] Margarida Borges,[1,5] Letícia Silva,[1] Ricardo Jorge Dinis-Oliveira,[6,7,8] Mariana Resende,[3,4] Margarida Correia-Neves,[3,4] Michael B. Jordan,[9] Nuno C. Ferreira,[10] Antero J. Abrunhosa[10] and Ricardo Silvestre[1,3,4]

[1]*Institute for Molecular and Cell Biology (IBMC), University of Porto, Porto, Portugal,* [2]*Departamento de Ciências Biológicas, Faculdade de Farmácia, Universidade do Porto, Porto, Portugal,* [3]*Life and Health Sciences Research Institute (ICVS), School of Health Sciences, University of Minho, Braga, Portugal,* [4]*ICVS/3Bs-PT Government Associate Laboratory, Braga/Guimarães, Portugal,* [5]*Department of Biological Sciences, Faculty of Pharmacy, University of Porto, Porto, Portugal,* [6]*Department of Legal Medicine and Forensic Sciences, Faculty of Medicine, University of Porto, Porto, Portugal,* [7]*Department of Sciences, IINFACTS – Institute of Research and Advanced Training in Health Sciences and Technologies, Advanced Institute of Health Sciences – North (ISCS-N), CESPU, CRL, Gandra, Portugal,* [8]*UCIBIO-REQUIMTE, Laboratory of Toxicology, Department of Biological Sciences, Faculty of Pharmacy, University of Porto, Porto, Portugal,* [9]*Department of Pediatrics, Cincinnati Children's Hospital Medical Center and University of Cincinnati College of Medicine, Cincinnati, OH, USA, and* [10]*Institute for Nuclear Sciences Applied to Health (ICNAS), University of Coimbra, Coimbra, Portugal*

doi:10.1111/imm.12464
Received 8 September 2014; revised 11 February 2015; accepted 13 March 2015.
Correspondence: Rui Appelberg, IBMC, Rua do Campo Alegre 823, Porto, Portugal. Email: rappelb@ibmc.up.pt
and
Ricardo Silvestre, ICVS, Campus de Gualtar, Braga, Portugal. Email: ricardosilvestre@ecsaude.uminho.pt
Senior author: Rui Appelberg

Summary

Granulomas are the hallmark of mycobacterial disease. Here, we demonstrate that both the cell recruitment and the increased glucose consumption in granulomatous infiltrates during *Mycobacterium avium* infection are highly dependent on interferon-γ (IFN-γ). *Mycobacterium avium*-infected mice lacking IFN-γ signalling failed to developed significant inflammatory infiltrations and lacked the characteristic uptake of the glucose analogue fluorine-18-fluorodeoxyglucose (FDG). To assess the role of macrophages in glucose uptake we infected mice with a selective impairment of IFN-γ signalling in the macrophage lineage (MIIG mice). Although only a partial reduction of the granulomatous areas was observed in infected MIIG mice, the insensitivity of macrophages to IFN-γ reduced the accumulation of FDG. *In vivo, ex vivo* and *in vitro* assays showed that macrophage activated by IFN-γ displayed increased rates of glucose uptake and *in vitro* studies showed also that they had increased lactate production and increased expression of key glycolytic enzymes. Overall, our results show that the activation of macrophages by IFN-γ is responsible for the Warburg effect observed in organs infected with *M. avium*.

Keywords: glycolysis; infection; interferon-γ; macrophages; mycobacteria.

Abbreviations: 2-NBDG, 2-[*N*-(7-nitrobenz-2-oxa-1,3-diazol-4-yl)amino]-2-deoxy-D-glucose; 7-AAD, 7-aminoactinomycin D; ATCC, American Type Culture Collection; FDG, fluorine-18-fluorodeoxyglucose; IFN-γ, interferon-γ; IL, interleukin; LDH, lactate dehydrogenase; MFI, mean fluorescence intensity; MIIG, macrophages insensitive to interferon-γ; PET, positron emission tomography

Introduction

The Warburg effect was first observed in cancer cells as an increase in the uptake of glucose and its transformation into lactate due to the enhanced use of glucose using the aerobic glycolytic pathway.[1,2] This same metabolic adaptation is also observed in immune cells during inflammation.[2] The increase in glucose uptake by cells performing glycolysis serves as the basis of positron emission tomography (PET) imaging using 2–[^{18}F]fluoro-2-deoxy-D-glucose (FDG).[3–5] In addition to its application in oncology, this technique is also being employed to visualize tuberculous lesions and follow their fate during chemotherapy.[6–9] Hence, mycobacterial granulomas also present increased utilization of glucose, most probably because of the use of glycolysis as the main metabolic pathway to produce ATP, so closely mimicking the metabolic changes observed in neoplastic tumours.[10,11]

Inflammatory macrophages have been known to up-regulate the glycolytic pathway to generate energy.[12,13] This up-regulation can be mediated by Toll-like receptor ligation but is not observed upon interleukin-4 (IL-4)/IL-13- or IL-10-mediated activation of macrophages.[14] Similarly, in dendritic cells stimulated with Toll-like receptor agonists and activated T cells, the ATP production and cellular survival are dependent on engaging the glycolytic pathway, with the majority of pyruvate being converted to lactate.[15–17]

The inflammatory reaction during mycobacterial infections is characterized by the structuring of granulomas.[18] Such lesions are characterized by a core predominantly made up of sessile macrophages and an outer cuff of motile lymphocytes.[19–21] Fibroblasts may form a capsule and neutrophils are seen in variable numbers. The course of infection may vary with the species and even the strain of the mycobacterial pathogen as well as the route of infection and the inoculum dose. We have studied in detail the response to an avian *Mycobacterium avium* strain that is highly virulent in certain mouse strains such as the C57BL/6 (B6) mouse.[22–25] When administered intravenously in low doses, *M. avium* ATCC 25291 produces focal lesions that increase progressively in size and eventually undergo central necrosis. In contrast, a high intravenous dose leads to a disseminated infection, with the early formation of granulomas but followed by the development of severe lymphopenia. The lesions in high-dose infections do not reach the same size observed with the low-dose infection although they tend to coalesce. Mice infected for more than 8 weeks with a high-dose inoculum have an extensive infiltration of the infected tissues with granulomas composed mostly of classically activated macrophages, so providing exuberant lesions to study.

Granulomas are believed to be poorly vascularized and should therefore represent a rather hypoxic environment.[20,26] Glycolysis would therefore allow energy generation in such low oxygen tension areas. However, little is known about the adaptation of leucocytes during granuloma formation and evolution. Here we show that both the size of the granulomas, i.e. the number of macrophages, and the activation of these phagocytes by interferon-γ (IFN-γ) determines the consumption of glucose via the glycolytic pathway.

Materials and methods

Mice

C57BL/6 (B6) mice were purchased from Charles River Laboratories (Barcelona, Spain). B6.IFN-$\gamma^{-/-}$ (IFN-γ-deficient) and B6.IFN-γR$^{-/-}$ (IFN-γ-R-deficient) mice were purchased from the Jackson Laboratories (Bar Harbor, ME) and bred in our animal facilities. B6 mice with macrophages insensitive to IFN-γ (MIIG mice)[27] were provided by Dr Michael Jordan and bred in our facilities. Animals were infected when 6–8 weeks old. Animal care and procedures were in accordance with institutional guidelines. This study was previously approved by the Portuguese National Authority for Animal Health – Direcção Geral de Veterinária.

Bacteria

Mycobacterium avium ATCC 25291 (from the American Type Culture Collection, Manassas, VA) forming smooth transparent colonies, was grown in supplemented Middlebrook 7H9 medium (Difco, Detroit, MI) containing 0·04% Tween-80 (Sigma Chemical Co., St Louis, MO) at 37° until the mid-log phase of growth. Bacteria were harvested by centrifugation and resuspended in a small volume of saline containing 0·04% Tween-80. The bacterial suspension was sonicated briefly with a Branson sonifier (Danbury, CT) to disrupt bacterial clumps, diluted and stored in aliquots at −70° until used. One aliquot was thawed at 37° and used to determine the concentration of mycobacteria in the inocula after plating serial dilutions of the suspension in a Middlebrook 7H10 agar medium (Difco) supplemented with oleic acid–albumin–dextrose–catalase. Before inoculation, bacterial aliquots were thawed at 37° and diluted in saline to the desired concentration.

In vivo infection

Mice were intravenously infected with 10^6 colony-forming units of *M. avium* ATCC 25291 through a lateral tail vein. Infected mice were killed at different time-points after infection.

In vivo glucose uptake

[^{18}F]FDG was synthesized according to previously described methods[28,29] on an IBA Synthera module (IBA,

Louvain-la-Neuve, Belgium). Animals were anaesthetized with ketamine plus medetomidine (50 + 0·5 mg/ml) intraperitoneally and injected with 2·5–5 MBq of [^{18}F] FDG in the tail vein. Images were acquired after an uptake period of 45 min using a high-resolution ClearPEM system (PETsys; Medical PET Imaging Systems, Oeiras, Portugal) with long LYSO crystals and depth-of-interaction information.[30] Image reconstruction was performed with interactive reconstruction (five iterations) with Gaussian smoothing at 1·2-mm spatial resolution. After the PET imaging, animals were killed and liver and spleen samples were collected and counted on a Capintec CRC-55tW well counter (Ramsey, NJ). Activity in these areas was quantified as percentage of injected activity per unit mass of tissue. For the flow cytometric evaluation of glucose uptake by single cells, *M. avium*-infected mice were injected intravenously with 500 μg of 2-[*N*-(7-nitrobenz-2-oxa-1,3-diazol-4-yl)amino]-2-deoxy-D-glucose (2-NBDG; Cayman Chemical, Ann Arbor, MI). Two hours later, spleen and liver tissues were removed and single-cell suspensions from each of those tissues were tested by flow cytometry for the presence of 2-NBDG. Splenic cell suspensions were obtained by gentle mechanical dissociation in PBS containing 10% fetal calf serum. Perfused livers were mashed on a 70-μm cell strainer to obtain a liver cell suspension, which was then resuspended in a 40% isotonic Percoll solution (GE Healthcare, Chalfont St Giles, UK) underlaid with an 80% isotonic Percoll solution. Hepatic mononuclear cells were isolated at the interface and washed twice in RPMI-1640 supplemented with 10% fetal calf serum. In both cell suspensions, erythrocytes were lysed using a haemolytic solution (155 mM NH_4Cl, 10 mM $KHCO_3$, pH 7·2). The number of viable cells was counted by trypan blue exclusion using the Countess™ automater cell counter (Invitrogen, Barcelona, Spain). After exclusion of debris and doublets the quantification of each population and their 2-NBDG uptake were analysed using a combination of markers in a FACSCanto II cytometer and analysed with FlowJo software; neutrophils ($CD11b^+$ $Ly6G^{hi}$ $NKp46^-$ $CD11c^-$), monocytes/macrophages ($CD11b^+$ $Ly6G^-$ $NKp46^-$ $CD11c^-$ $Ly6C^{int/+}$ $F4/80^+$), conventional dendritic cells ($CD11c^{hi}$ $Ly6C^-$ $Ly6G^-$ $MHCII^{high}$), CD4 T cells ($CD3^+$ $CD4^+$), CD8 T cells ($CD3^+$ $CD8^+$) and B cells ($CD3^-$ $CD19^+$).

In vitro bone marrow macrophage differentiation and infection

Bone marrow was recovered from the femurs of C57BL/6 mice and bone marrow-derived macrophages were obtained by cultivating cells for 7 days with 5% L-929 cell-derived culture medium in Dulbecco's modified Eagle's medium (Lonza, Basel, Switzerland) with 10% fetal bovine serum (Gibco, Grand Island, NY). Differentiated bone marrow-derived macrophages were infected with *M. avium* ATCC 25291 at a multiplicity of infection of 2 and/or treated with recombinant IFN-γ.

In vitro glucose uptake assay

Uninfected or *M. avium*-infected cells treated or not with recombinant IFN-γ (100 units/ml; Genzyme, Cambridge, MA) were incubated with 90 μM of 2-NBDG (Cayman Chemical), a fluorescent analogue of glucose, in Dulbecco's modified Eagle's medium supplemented medium without glucose for 1 hr at 37°. Cells were washed twice with cold PBS, harvested and stained with 1 μg/ml of 7-aminoactinomycin D (7-AAD) (Sigma, St Louis, MO). The 2-NBDG uptake was quantified on live ($7\text{-}AAD^-$) bone marrow-derived macrophages in a FACSCanto II cytometer and analysed with FlowJo software. Peritoneal macrophages isolated by peritoneal lavage from infected mice were processed *in vitro* as indicated above in one experiment.

Quantitative PCR analysis

Total RNA was isolated from cells with TRIzol reagent (Invitrogen) according to the manufacturer's instructions. Total RNA was reverse-transcribed using the iScript Select cDNA Synthesis Kit (Bio-Rad, Hercules, CA) and real-time quantitative PCR were run in triplicate for each sample on a Bio-Rad My Cycler iQ5 (Bio-Rad). Primer sequences were obtained from Stabvida (Costa da Caparica, Portugal) and thoroughly tested. The resulting RT product was expanded using the Syber Green Supermix (Bio-Rad). The results were then normalized to the expression of a housekeeping gene *Srp72*. After amplification, a threshold was set for each gene and cycle threshold-values (Ct-values) were calculated for all samples. Gene expression changes were analysed using the built-in iQ5 Optical system software v2.1 (Bio-Rad). The complete list of primers used is given in Table 1.

Quantification of LDH activity and secreted lactate

The reagents for lactate dehydrogenase (LDH) and lactate were obtained from PZ Cormay S.A. LDH (from cell lysates) and lactate (from culture supernatants) were measured on an AutoAnalyzer (PRESTIGE 24i, PZ Cormay S.A.). Briefly, lactate dehydrogenase (LDH) catalyses the reduction of pyruvate by NADH, according to the following reaction: Pyruvate + NADH + H^+ → L-lactate + NAD^+. The rate of decrease in concentration of NADPH, was measured photometrically at 340 nm, and it is proportional to the catalytic concentration of LDH present in the sample. Lactate is oxidized by lactate oxidase to pyruvate and hydrogen peroxide which, in the presence of peroxidase, reacts with *N*-ethyl-*N*-(2-hydroxy-3-sulfopropyl)-3-methylaniline forming a red compound, the

Table 1. List of primers used for quantitative PCR

Genes	Forward sequence	Reverse sequence
Pdk1	GGACTTCGGGTCAGTGAATGC	TCCTGAGAAGATTGTCGGGGA
Pkm2	TTGCAGCTATTCGAGGAACTCCG	CACGATAATGGCCCCACTGC
Ldha	TGTCTCCAGCAAAGACTACTGT	GACTGTACTTGACAATGTTGGGA
Slc2a1	CCAGCTGGGAATCGTCGTT	AAGTCTGCATTGCCCATGAT
HkI	CGGAATGGGGAGCCTTTGG	GCCTTCCTTATCCGTTTCAATGG
HkII	TGATCGCCTGCTTATTCACGG	AACCGCCTAGAAATCTCCAGA
Srp72	CACCCAGCAGACAGACAAACTG	GCACTCATCGTAGCGTTCCA

Table 2. Accumulation of 18-fluorodeoxyglucose in the livers and spleens of *Mycobacterium avium*-infected mice (percentage of injected activity per unit mass of tissue)

	Liver	Spleen
Uninfected mice ($n = 6$)	1·3 ± 0·5	2·1 ± 0·6
Infected B6 ($n = 11$)	15·2 ± 4·6 1	13·8 ± 5·63
Infected IFN-γ-deficient ($n = 13$)	2·8 ± 0·7	8·1 ± 1·84
Infected MIIG ($n = 5$)	7·8 ± 2·5 2	8·4 ± 2·4

The values are expressed as percentage of injected activity per tissue mass unit. The mean and standard deviation are shown and the number of animals used is given in parenthesis. For the liver, statistically significant differences were $^1P < 0{\cdot}001$ between infected B6 and uninfected mice and between infected IFN-γ-deficient and infected B6 mice. $^2P < 0{\cdot}05$ between uninfected mice and infected mice with macrophages insensitive to interferon-γ (MIIG). For the spleen, statistical differences were $^3P < 0{\cdot}01$ between infected B6 and uninfected mice and $^4P < 0{\cdot}05$ between infected IFN-γ-deficient and uninfected mice.

Table 3. Analysis of the degree of inflammatory infiltration in livers of *Mycobacterium avium*-infected mice

Mouse strain	B6	IFN-γR-deficient	MIIG
Experiment 1 (90 dpi)	49·4 ± 6·6	6·9 ± 1·6*	–
Experiment 2 (74 dpi)	44·1 ± 7·6	–	31·5 ± 15·6
Experiment 3 (80 dpi)	64·5 ± 7·6	–	23·5 ± 3·1

Haematoxylin & eosin stained sections were photographed and the area of inflammatory infiltration was quantified as percentage of the total section area.

The values are expressed as percentage of infiltrated area in the total area of the liver. The mean and standard deviation are shown. Four mice per group were studied. Statistically significant differences were $^*P < 0{\cdot}01$ between infected B6 and infected IFN-γ-deficient mice. –, not done; MIIG, macrophages insensitive to interferon-γ; IFN-γ, interferon-γ.

colour intensity of which, measured at 546 and 700 nm, is proportional to the concentration of lactate in the examined sample.

Statistical analysis

For comparing multiple groups (Tables 2 and 3) a Kruskal–Wallis test was performed to assess differences between the measures taken for the different groups. When differences were indeed detected, *post hoc* tests (Dunn's tests) were performed to assess which pairs of groups differed. Analysis of data from Figures 2–4 was performed using the one-way analysis of variance test with a Bonferroni multiple-comparison post-test for multiple group comparisons. Statistically significant values are as follows: $^*P < 0{\cdot}05$, $^{**}P < 0{\cdot}01$, $^{***}P < 0{\cdot}001$.

Results

We used a PET scanning device typically applied to human patients for the imaging of the mammary gland following administration of positron-emitting substrates and their uptake by a possible neoplastic lesion. The size of the device lends itself to the analysis of small rodents and other small animals. B6 mice and IFN-γ-deficient mice were infected intravenously with the virulent *M. avium* strain ATCC 25291. After 75 days of infection, the mice were anaesthetized and given an intravenous bolus of FDG. A group of uninfected mice was similarly treated. After a 45-min period to allow virtually complete uptake of FDG (or its elimination by glomerular filtration), mice were submitted to PET scanning and the images were subsequently processed as described above. As shown in Fig. 1, non-infected mice showed most of the labelled FDG accumulating in the bladder and in the brain whereas infected B6 animals showed intense labelling of the liver and spleen. In contrast, IFN-γ-deficient mice had no labelling of that area and instead had most of the FDG accumulating in the bladder and some in the brain.

To quantify the accumulation of FDG in the liver and spleen of these mice, the organs were collected and the amount of gamma radiation emitted was quantified. As shown in Table 2, uninfected mice exhibited minimal accumulation of FDG in either the spleen or the liver. Infected B6 mice presented higher labelling by FDG in

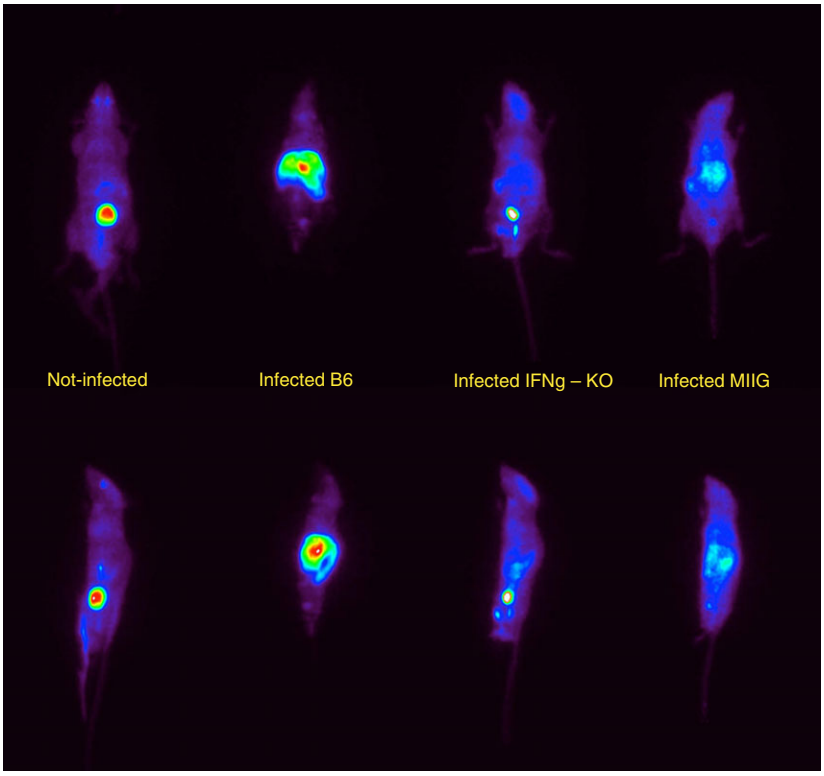

Figure 1. *Mycobacterium avium* infected mice show an interferon-γ (IFN-γ)-dependent Warburg effect in the liver and spleen. 18-Fluorodeoxyglucose (FDG) positron emission tomography stack of coronal and sagittal section images (nose in the top, tail in the bottom) of non-infected mice (left) or B6 (second from the left), IFNγ-deficient (third from the left), and macrophages insensitive to interferon-γ (MIIG) (right) mice infected for 75 days with 10^6 CFU of *M. avium* ATCC 25291.

both organs as compared with uninfected animals ($P < 0{\cdot}001$ in both organs). In contrast, the labelling in the liver of IFN-γ-deficient mice was close to that in non-infected mice (not statistically different) and so was much lower than in infected wild-type animals ($P < 0{\cdot}001$). The labelling of the spleen in infected IFN-γ-deficient mice was intermediate between that in non-infected mice and infected B6 mice ($P < 0{\cdot}05$ when compared with the former).

To address the role played by macrophage activation mediated by IFN-γ, we studied FDG accumulation in mice with macrophages insensitive to IFN-γ activation (MIIG, see ref. [27]). PET scans revealed low labelling of the liver and spleen (Fig. 1) but quantification of FDG uptake showed that it was significantly increased in the liver when compared with uninfected animals but reduced in both organs relative to that seen in infected B6 animals although the differences were not statistically significant (Table 2). FDG accumulation in the spleen of MIIG mice was not statistically different from that observed in the other mice. These data show that increased glucose consumption may occur in the absence of macrophage activation.

Macrophages are the predominant cell type in granulomas and their number may affect the total amount of FDG captured by the infected organs. We therefore compared the size of granulomas in infected mice in which no cell responds to IFN-γ (IFN-γ-receptor-deficient mice), mice in which macrophages do not respond to the cytokine (MIIG mice) and wild-type controls. Histological analysis of the liver showed that granulomatous areas remain drastically reduced in the total absence of IFN-γ signalling when compared with wild-type hosts, even at long periods of infection such as the one shown in Table 3. In contrast to IFN-γ-R-deficient animals, MIIG mice showed a much smaller reduction in inflammatory infiltration when compared with B6 mice (Table 3). Representative images of liver sections are provided in the Supplementary material (Figure S1). Granulomas in MIIG mice presented a higher number of lymphocytes than granulomas in B6 control mice, suggesting that T and B cells could contribute to the enhanced accumulation of FDG in MIIG organs (Figure S1). Histological and microbiological data in IFN-γ-deficient mice were the same as in IFN-γ-R-deficient mice (data not shown).

Given that mice whose macrophages fail to respond to and be activated by IFN-γ also have different cellular compositions of the granulomas, we quantified the number of leucocytes in infected organs (spleen and liver) of mice and we assessed whether macrophage activation played a role in the increased uptake of glucose seen *in vivo*. For the latter we used *in vivo, ex vivo* and *in vitro* assays.

At day 70 of infection, the number of $CD4^+$ T cells, macrophages and neutrophils were increased in B6 and MIIG mice compared with non-infected controls and the numbers of B cells and dendritic cells were significantly increased in B6 mice (Fig. 2). In the liver, T cells were in

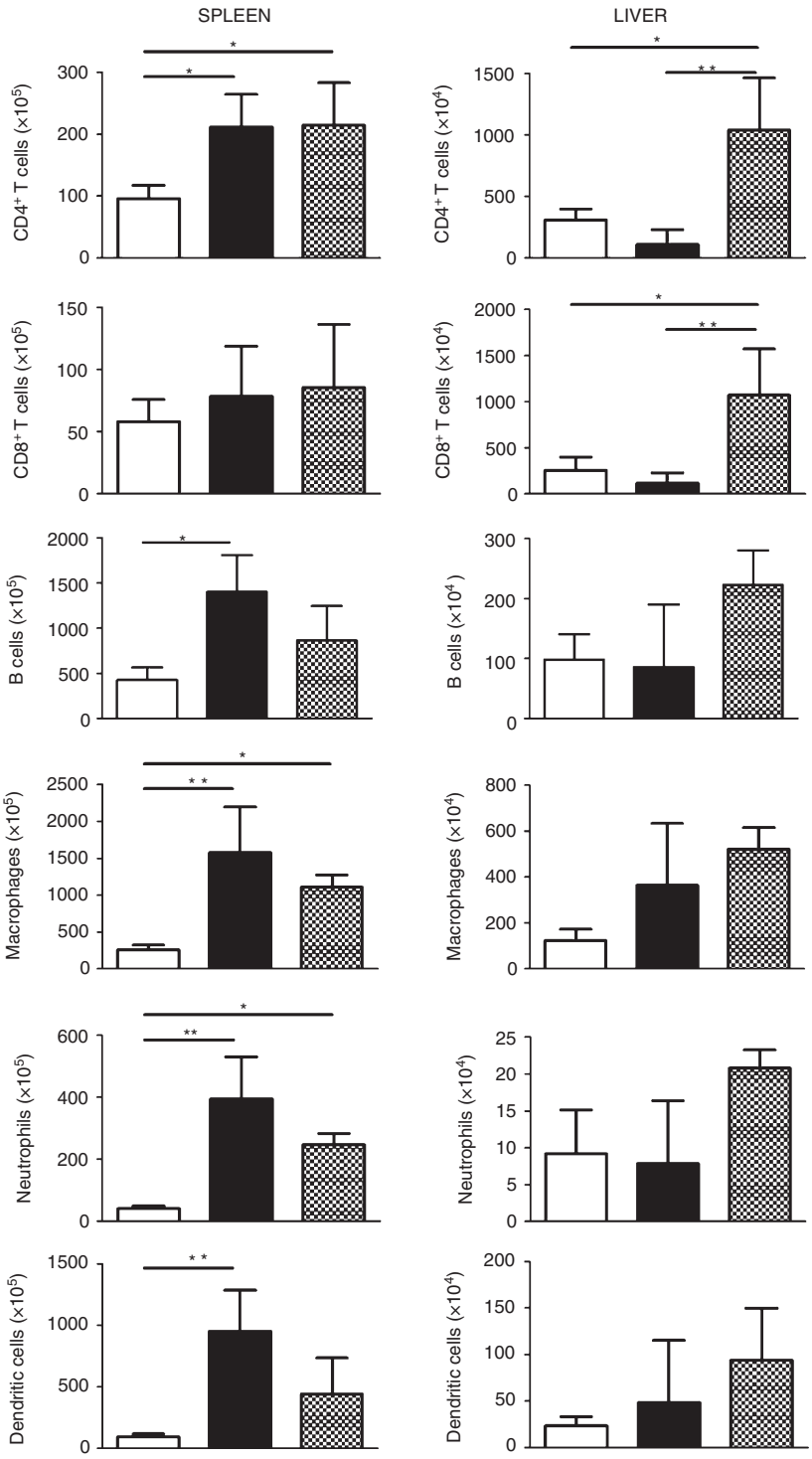

Figure 2. Quantification of immune cell infiltrates in *Mycobacterium avium*-infected mice. Seventy days after *M. avium* infection, spleen and liver cells from non-infected mice (white bars) or B6 (solid black bars) and macrophages insensitive to interferon-γ (MIIG) (solid square bars) infected mice were stained with specific antibodies and analysed by flow cytometry. Each bar represents the mean $\pm$ SD from four to five animals per group. $^{*}P < 0{\cdot}05$, $^{**}P < 0{\cdot}01$.

significantly greater numbers in infected MIIG mice compared with non-infected or infected B6 animals (Fig. 2). Increased uptake of 2-NBDG relative to non-infected mice was only observed in macrophages from infected B6 mice (Fig. 3). This increase was not observed in macrophages from MIIG mice. All other cell types showed similar uptake independent of being isolated from infected or non-infected mice and regardless of the strain (Fig. 3). In one experiment, peritoneal macrophages from infected mice were cultured *in vitro* with 2-NBDG and the uptake of the compound was analysed by flow cytometry. Macrophages from non-infected animals showed a mean fluorescence intensity (MFI) of $2446{\cdot}7 \pm 431{\cdot}1$ whereas a significant increase of 2-NBDG uptake was

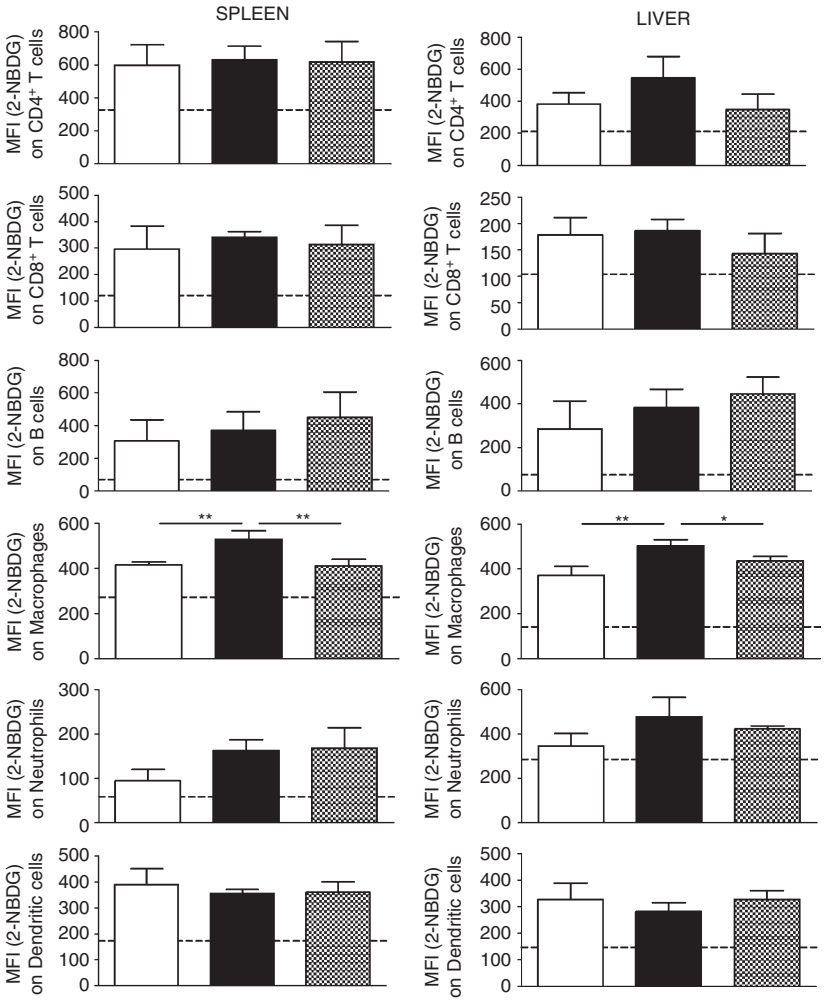

Figure 3. Enhanced glycolytic activity in liver and splenic macrophages of *Mycobacterium avium*-infected mice. *In vivo* glucose uptake of spleen and liver immune cell populations of non-infected mice (white bars) or B6 (solid black bars) and macrophages insensitive to interferon-γ (MIIG) (solid square bars) infected mice was measured using a fluorescent D-glucose analogue (2-NBDG). As a control sample for *in vivo* experiments, mice that did not receive 2-NBDG were analysed (dashed line). Mean fluorescence intensity (MFI) of 2-NBDG in each cell population is indicated. Mean $\pm$ SD were obtained from four to five mice in each condition. $^*P < 0{\cdot}05$, $^{**}P < 0{\cdot}01$.

observed in macrophages from infected B6 mice (MFI of $5035{\cdot}4 \pm 1202{\cdot}5$). Macrophages from infected MIIG mice showed reduced accumulation of 2-NBDG relative to the latter (MFI of $2780{\cdot}7 \pm 726{\cdot}5$).

To further test the role of macrophage activation in the increase in the uptake of glucose, we cultured macrophages and exposed them to infection, IFN-γ or both and analysed several parameters to characterize their metabolic activity. As shown in Fig. 4(a), IFN-γ activation of macrophages led to the increased expression of the genes encoding key glycolytic enzymes and transporters, namely hexokinases 1 (*Hk1*) and 2 (*Hk2*), pyruvate kinase isoenzyme 2 (*Pkm2*), pyruvate dehydrogenase lipoamide kinase isozyme 1 (*Pdk1*), SLC2A1 glucose transporter 1 (*Slc2a1*) and lactate dehydrogenase A (*Ldha*). Infection alone, in the conditions used, did not up-regulate the expression of these genes nor affect the effects of IFN-γ. The IFN-γ-induced increase in expression of *Ldha* was accompanied by an increase in the enzymatic activity of LDH (Fig. 4b) as well as an increase in the accumulation of lactate in the culture medium (Fig. 4c). Interferon-γ-treated macrophages also exhibited an increase in the accumulation of the fluorescent deoxyglucose analogue 2-NBDG, mimicking the *in vivo* observations (Fig. 4d).

Discussion

The phenomenon of increased glucose utilization through aerobic glycolysis described by Warburg in neoplastic cells has been later found to occur in immune cells.[2] Macrophages were known for a long time to resort to this type of metabolism and recent research has been uncovering a complex network of metabolic adaptations in lymphocytes, namely the switch from aerobic respiration to aerobic glycolysis.[17] The imaging of granulomas in tuberculosis through PET scanning of hosts (human or animal) treated with FDG has been used to stage the severity of the disease and assess the efficacy of antimicrobial therapy.[6,8] Here we show that the accumulation of the glucose analogue in infected tissues depends on the action of IFN-γ. This cytokine is pivotal in the recruitment of cells into granulomas, namely macrophages, and a major activator of the latter cells. We observed that both activities of IFN-γ are important for the induction of the War-

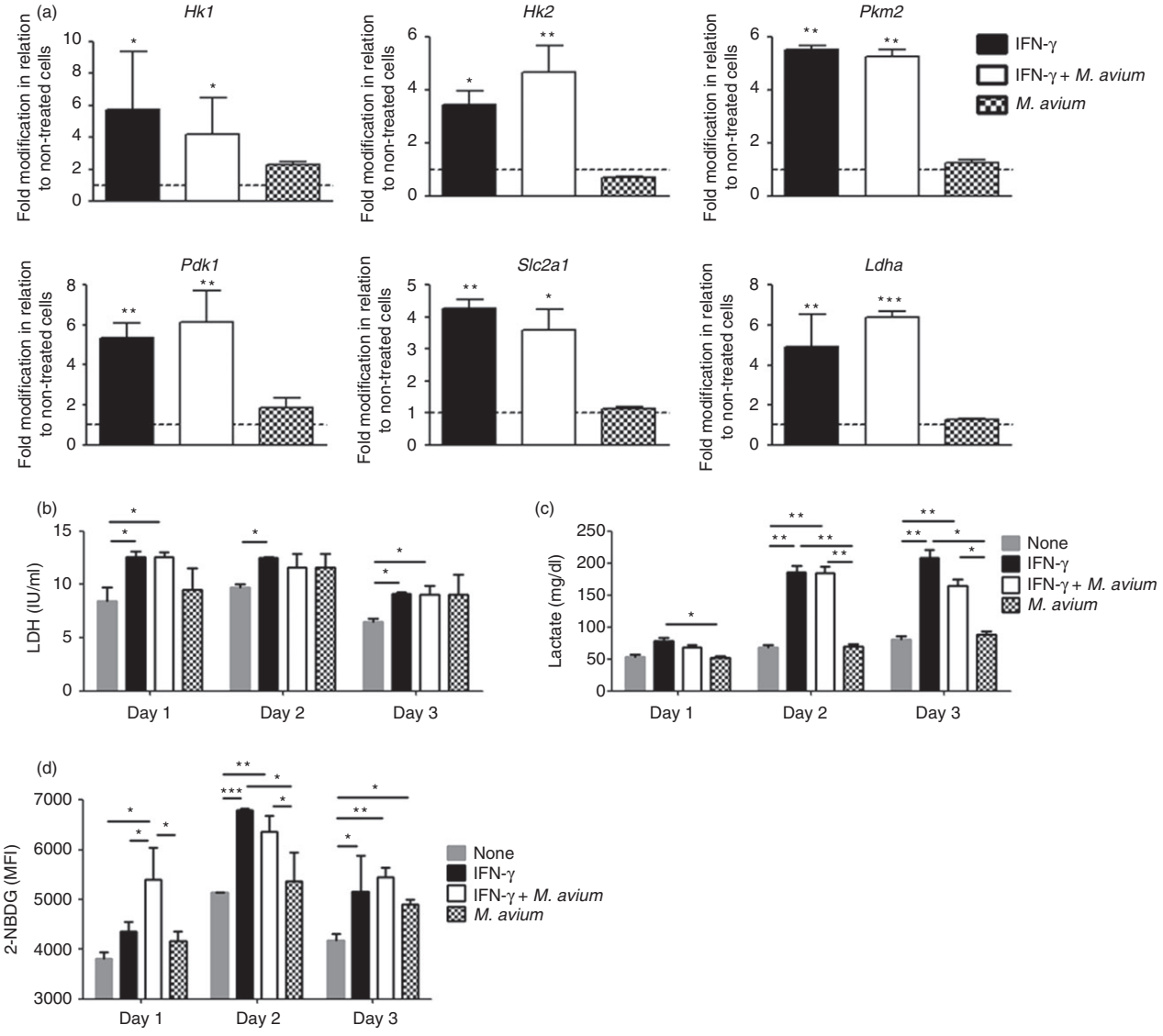

Figure 4. *Mycobacterium avium*-infected macrophages exposed to interferon-γ (IFN-γ) display increased rate of glucose uptake and aerobic glycolysis. Bone marrow-derived macrophages were infected with *M. avium* ATCC 25291 and/or treated with IFN-γ (100 U/ml). The transcription profile of key glycolytic enzymes was evaluated after 24 hr (a). Levels of intracellular lactate dehydrogenase (LDH) activity (b) and extracellular lactate (c) were measured during the 3 days following infection and/or treatment. The levels of glucose uptake (2-NBDG uptake, mean fluorescence intensity) were quantified by flow cytometry during the 3 days following infection and/or treatment (d). Means ± SD are from three independent experiments. $*P < 0{\cdot}05$, $**P < 0{\cdot}01$, $***P < 0{\cdot}001$.

burg effect. In the total absence of IFN-γ signalling, the hepatic accumulation of macrophages in granulomas is drastically reduced and the accumulation of FDG is minimal. In the case of partial interference with IFN-γ signalling, i.e. when only macrophages fail to respond to the cytokine, PET scans revealed a marked reduction in FDG accumulation. Isotope quantification showed that the organs of MIIG mice still presented an increase in the uptake of FDG. The histological analysis of the hepatic lesions in these mice showed the presence of a large granulomatous infiltration of the tissues and an increase in the number of lymphocytes around the granulomas. By performing a flow cytometric analysis of the uptake of a fluorescent deoxy-glucose analogue we showed that only macrophages respond to IFN-γ with an increase in this uptake whereas the contribution of lymphocytes is related to their total number, which is increased in the infected mice and particularly so in the livers of infected MIIG mice. Hence, in the absence of macrophage activation we still observe proper formation of granulomas while lymphocyte survival or expansion is higher, as already published[24] and so the FDG or 2-NDBG uptake in the organs of MIIG mice is still relevant because of the activity of the more numerous lymphocytes.

In vitro assays confirmed that IFN-γ is able to increase the activity of the aerobic glycolytic pathway by increasing the expression of key enzymes and ultimately of LDH, leading to the reduction of pyruvate to lactate and consequently of secretion of the latter.[14,31] Hence, both increased recruitment of macrophages and increased glycolytic activity of these phagocytes are regulated by IFN-γ, leading to the observed Warburg effect.

One pertinent issue concerning the metabolic adaptations of granuloma macrophages is the effect they may have on lymphocytes that circulate through these lesions. Indeed, lymphocytes are not only important for the proper structuring of a mature granuloma but they remain associated, at least transiently, throughout the life of this structure. It has been shown that the accumulation of lymphocytes in *M. avium*-induced granulomas is higher in hosts that are deficient in the inducible form of nitric oxide synthase than in control animals.[32] Hence, the corollary of lymphocyte functions, namely the activation of macrophages in the granuloma, has a negative effect on the activity of these cells. Nothing is known about the consequences of the activation of aerobic glycolysis in granuloma macrophages on lymphocyte activity. Lactate itself may depress T-cell function and induce cell death in terminally differentiated T cells,[33] which, in association with poor presentation of mycobacterial antigens by granuloma macrophages,[34] may limit the efficacy of lymphocytes in the granuloma milieu. In addition, as actively proliferating cells, both $CD4^+$ and $CD8^+$ effector T cells engage in aerobic glycolysis irrespective of the oxygen availability.[35] Inside the granuloma microenvironment, T cells should compete with macrophages, which are avid glucose consumers, for its availability. This competitive model of glucose restriction may selectively impact T effector cells contributing to pathogen persistence. In conclusion, the current work demonstrates the crucial role of IFN-γ acting on macrophages for the Warburg effect observed in the mycobacterial granuloma.

Acknowledgements

The authors are grateful to M. Patrício for statistical analysis and to V. Alves and J. Rio for technical support. This work was funded by project 'NORTE-07-0124-FEDER-000002-Host-Pathogen Interactions' co-funded by Programa Operacional Regional do Norte (ON.2—O Novo Norte), under the Quadro de Referência Estratégico Nacional (QREN), through the Fundo Europeu de Desenvolvimento Regional (FEDER) and by Fundação para a Ciência e Tecnologia.

Disclosures

The authors declare no competing interests of this work.

References

1 Warburg O, Wind F, Negelein E. The metabolism of tumors in the body. *J Gen Physiol* 1927; **8**: 519–30.
2 Palsson-McDermott EM, O'Neill LAJ. The Warburg effect then and now: from cancer to inflammatory diseases. *BioEssays* 2013; **35**:965–73.
3 Schmidt KC, Lucignami G, Sokoloff L. Fluorine-18-Fluorodeoxyglucose PET to determine regional cerebral glucose utilization: a re-examination. *J Nucl Med* 1996; **37**: 394–9.
4 Gotthardt M, Bleeker-Rovers CP, Boerman OC, Oyen WJG. Imaging of inflammation by PET, conventional scintigraphy, and other imaging techniques. *J Nucl Med* 2010; **51**:1937–49.
5 Burrows RC, Freeman SD, Charlop AW, Wiseman RW, Adamsen TCH, Krohn KA, Spence AM. [^{18}F]-2-fluoro-2-deoxyglucose transport kinetics as a function of extracellular glucose concentration in malignant glioma, fibroblast and macrophage cells *in vitro*. *Nucl Med Biol* 2004; **31**:1–9.
6 Hofmeyr A, Eddie Lau WF, Slavin MA. *Mycobacterium tuberculosis* infection in patients with cancer, the role of 18-fluorodeoxyglucose positron emission tomography for diagnosis and monitoring treatment response. *Tuberculosis* 2007; **87**:459–63.
7 Kim IJ, Lee JS, Kim S-J, Kim Y-K, Jeong YJ, Jun S, Nam HY, Kim JS. Double-phase ^{18}F-FDG Pet-CT for determination of pulmonary tuberculoma activity. *Eur J Nucl Med Mol Imaging* 2008; **35**:808–14.
8 Davis SL, Nuermberger EL, Um PK, Vidal C, Jedynak B, Pomper MG, Bishai WR, Jain SK. Noninvasive pulmonary [^{18}F]-2-Fluoro-deoxy-D-glucose positron emission tomography correlates with bactericidal activity of tuberculosis drug treatment. *Antimicrob Agents Chemother* 2009; **53**:4879–84.
9 Via LE, Schimel D, Weiner DM *et al.* Infection dynamics and response to chemotherapy in a rabbit model of tuberculosis using [^{18}F]2-fluoro-deoxy-D-glucose positron emission tomography and computed tomography. *Antimicrob Agents Chemother* 2012; **56**:4391–402.
10 Somashekar BS, Amin AG, Rithner CD, Troudt J, Basaraba R, Izzo A, Crick DC, Chatterjee D. Metabolic profiling of lung granuloma in *Mycobacterium tuberculosis* infected guinea pigs: *ex vivo* 1H magic angle spinnng NMR studies. *J Proteome Res* 2011; **10**:4186–95.
11 Mehrotra P, Jamwal SV, Saquib N, Sinha N, Siddiqui Z, Manivel V, Chatterjee S, Rao KV. Pathogenicity of *Mycobacterium tuberculosis* is expressed by regulating metabolic thresholds of the host macrophage. *PLoS Pathog* 2014; **10**:e1004265.
12 Newsholme P, Curi R, Gordon S, Newsholme EA. Metabolism of glucose, glutamine, long-chain fatty acids and ketone bodies by murine macrophages. *Biochem J* 1986; **239**:121–5.
13 McGettrick AF, O'Neill LAJ. How metabolism generates signals during innate immunity and inflammation. *J Biol Chem* 2013; **288**:22893–7.
14 Rodriguez-Prados J-C, Través PG, Cuenca J, Rico D, Aragonés J, Martin-Sanz P, Cascante M, Boscá L. Substrate fate in activated macrophages: a comparison between innate, classic, and alternative activation. *J Immunol* 2010; **185**:605–14.
15 Krawczyk CM, Holowka T, Sun J *et al.* Toll-like receptor-induced changes in glycolytic metabolism regulate dendritic cell activation. *Blood* 2010; **115**:4742–9.
16 Wang R, Green DR. Metabolic checkpoints in activated T cells. *Nat Immunol* 2012; **13**:907–15.
17 Pearce EL, Pearce EJ. Metabolic pathways in immune cell activation and quiescence. *Immunity* 2013; **38**:633–43.
18 Shaler CR, Horvath CN, Jeyanathan M, Xing Z. Within the Enemy's Camp: contribution of the granuloma to the dissemination, persistence and transmission of *Mycobacterium tuberculosis*. *Front Immunol* 2013; **4**:30.
19 Gonzalez-Juarrero M, Turner OC, Turner J, Marietta P, Brooks JV, Orme IM. Temporal and spatial arrangement of lymphocytes within lung granulomas induced by aerosol infection with *Mycobacterium tuberculosis*. *Infect Immun* 2001; **69**:1722–8.
20 Tsai MC, Chakravarty S, Zhu G *et al.* Characterization of the tuberculous granuloma in murine and human lungs: cellular composition and relative tissue oxygen tension. *Cell Microbiol* 2006; **8**:218–32.
21 Egen JG, Rothfuchs AG, Feng CG, Winter N, Sher A, Germain RN. Macrophage and T cell dynamics during the development and disintegration of mycobacterial granulomas. *Immunity* 2008; **28**: 271–84.
22 Appelberg R, Castro AG, Pedrosa J, Silva RA, Orme IM, Minóprio P. The role of gamma interferon and tumor necrosis factor-alpha during the T cell independent and dependent phases of *Mycobacterium avium* infection. *Infect Immun* 1994; **62**: 3962–71.
23 Flórido M, Gonçalves AS, Silva RA, Ehlers S, Cooper AM, Appelberg R. Resistance of virulent *Mycobacterium avium* to interferon-γ-mediated antimicrobial activity suggests additional signals for induction of mycobacteriostasis. *Infect Immun* 1999; **67**:3610–8.
24 Flórido M, Pearl JE, Solache A, Borges M, Haynes L, Cooper AM, Appelberg R. Gamma interferon-induced T cell loss in virulent *Mycobacterium avium* infection. *Infect Immun* 2005; **73**:3577–86.

25 Flórido M, Cooper AM, Appelberg R. Immunological basis of the development of necrotic lesions following *Mycobacterium avium* infection. *Immunology* 2002; **106**:590–601.
26 Aly S, Wagner K, Keller C, Malm S, Malzan A, Brandau S, Bange FC, Ehlers S. Oxygen status of lung granulomas in *Mycobacterium tuberculosis*-infected mice. *J Pathol* 2006; **210**:298–305.
27 Lykens JE, Terrell CE, Zoller EE *et al.* Mice with a selective impairment of IFN-γ signaling in macrophage lineage cells demonstrate the critical role of IFN-γ-activated macrophages for the control of protozoan parasitic infections *in vivo*. *J Immunol* 2010; **184**:877–85.
28 Hamacher K, Coennen HH, Stoecklin G. Efficient stereospecific synthesis of no-carrier-added 2-[F-18]-fluoro-2-deoxy-D-glucose using aminopolyether supported nucleophilic substitution. *J Nucl Med* 1986; **27**:235–8.
29 Abrunhosa AJ, Alves F, Oxley I, Boumon R, Gameiro C. Optimization of [^{18}F]-FDG production with terminal sterilization by autoclave. *J Nucl Med* 2012; **53**:524.
30 Abreu MC, Aguiar JD, Almeida FG *et al.* Design and evaluation of the Clear-PEM scanner for positron emission mammography. *IEEE Trans Nucl Sci* 2006; **53**:71–7.
31 Garedew A, Moncada S. Mitochondrial dysfunction and HIF1α stabilization in inflammation. *J Cell Sci* 2008; **121**:3468–75.
32 Gomes MS, Flórido M, Pais TF, Appelberg R. Improved clearance of *Mycobacterium avium* upon disruption of the iNOS gene. *J Immunol* 1999; **162**:6734–9.
33 Fischer K, Hoffmann P, Voekl S *et al.* Inhibitory effect of tumor cell-derived lactic acid on human T cells. *Blood* 2007; **109**: 3812–9.
34 Egen JG, Rothfuchs AG, Feng CG, Horwitz MA, Sher A, Germain RN. Intravital imaging reveals limited antigen presentation and T cell effector function in mycobacterial granulomas. *Immunity* 2011; **34**:807–19.
35 Pearce EL, Poffenberger MC, Chang CH, Jones RG Fueling immunity: insights into metabolism and lymphocyte function. *Science* 2013; **342**: 1242454. doi: 10.1126/science.1242454.

Supporting Information

Additional Supporting Information may be found in the online version of this article:

Figure S1. Representative haematoxylin & eosin-stained sections of liver tissues from B6 (A), interferon-γ-R-deficient (B) and macrophages insensitive to interferon-γ (MIIG) (C) mice.